Journal of Alloys and Compounds 507 (2010) 297–301

Contents lists available at ScienceDirect

Journal of Alloys and Compounds

journal homepage: www.elsevier.com/locate/jallcom

Characterization and magnetic properties of $Ba_xSr_{1-x}Fe_{12}O_{19}$ (x = 0–1) ferrite hollow fibers via gel-precursor transformation process

Fuzhan Song [a], Xiangqian Shen [a,*], Jun Xiang [a], Yongwei Zhu [b]

[a] School of Material Science and Engineering, Jiangsu University, Zhenjiang 212013, China
[b] School of Mechanical and Electrical Engineering, Nanjing University of Aeronautics and Astronautics, Nanjing 210016, China

ARTICLE INFO

Article history:
Received 21 November 2009
Received in revised form 28 July 2010
Accepted 29 July 2010
Available online 4 August 2010

Keywords:
Ferrite
$Ba_xSr_{1-x}Fe_{12}O_{19}$
Hollow fibers
Magnetic property

ABSTRACT

The $Ba_xSr_{1-x}Fe_{12}O_{19}$ (x = 0–1) ferrite hollow fibers with diameters of 1 to 2 μm have been prepared by the gel-precursor transformation process. The gel-precursor decomposition and ferrite formation were analyzed by thermo-gravimetric and differential scanning calorimetry, infrared spectroscopy and X-ray diffraction. The $Ba_xSr_{1-x}Fe_{12}O_{19}$ ferrite hollow fibers as-prepared were characterized with scanning electron microscopy and vibrating sample magnetometer. The results show that the $Ba_xSr_{1-x}Fe_{12}O_{19}$ (x = 0–1) ferrite hollow fibers are of a solid solution and these fibers with an obvious hollow structure consist of fine hexagonal plate-like particles. Their magnetic properties are mainly influenced by the chemical composition and grain size. With the barium substitution, the specific saturation magnetization and coercivity of the $Ba_xSr_{1-x}Fe_{12}O_{19}$ ferrite hollow fibers decrease from 67.1 Am^2/kg and 443.3 kA/m (for the simple $SrFe_{12}O_{19}$ ferrite, x = 0) to 56.1 $A\,m^2/kg$ and 319.8 kA/m (for the simple $BaFe_{12}O_{19}$ ferrite, x = 1.0), respectively. The $Ba_{0.5}Sr_{0.5}Fe_{12}O_{19}$ ferrite hollow fibers calcined at 1000 °C for 2 h are composed of single-domain grains around 60 nm and exhibit the specific saturation magnetization 63.9 $A\,m^2/kg$ and coercivity 416.5 kA/m.

1. Introduction

The hexagonal ferrites with a magnetoplumbite structure and a general formula $MFe_{12}O_{19}$ (M = Ba, Sr) are well-known ceramic permanent magnets. They are widely used in magnetic recording and microwave devices owing to their high maximum saturation magnetization, appropriate Curie temperature, high theoretical maximum coercivity, high magneto-crystalline anisotropy and excellent chemical stability [1–3]. However, these hexagonal ferrites are quite heavy as in bulk ceramic materials, which limit their applications in many high-tech fields.

In order to reduce the specific density, short fibers with a high aspect ratio have attracted materials scientists and engineers. The investigations proved that fibers could bring a much higher magnetic permeability than the same volume of materials in a non-fibrous form [4,5]. Fibrous forms of ceramic materials could also be made stronger and often stiffer in mechanics than the bulk ceramic. If the hexagonal ferrites are made into fibers and in particular hollow fibers, the ferrite hollow fibers will have a low specific density owing to a large specific surface area and exhibit some unique characteristics.

The commercial hexagonal ferrites usually possess a large grain size of multi-domains [6]. For a magnetically optimized hexagonal ferrite a grain size of single-domain is required, with 80% of the theoretical maximum coercivity reported for grains of 0.1 μm [1]. In order to obtain highly homogeneous single-domain hexagonal ferrites, several techniques have been developed, such as citrate-precursor [7,8], chemical co-precipitation [9], glass-crystallization [10], micro-emulsion [11,12], self-propagate [13] and hydrothermal [14,15] methods. But, these preparative routes are mainly focused on the hexagonal ferrite powders, a few reports on the fibers. Gong et al. [16] reported the preparation of barium ferrite hollow fibers by the aqueous sol–gel process. Pullar and Bhattacharya [17] synthesized the barium ferrite fibers and strontium ferrite fibers by the organic gel method. However, the formation process and relation between the structure and magnetic characteristics for these fibers are not fully understood. As there is no reports on solid solution of barium and strontium ferrite fibers, the aim of this investigation therefore is to determine the feasibility of utilizing the gel-precursor transformation process to prepare the $Ba_xSr_{1-x}Fe_{12}O_{19}$ (x = 0–1) ferrite hollow fibers, characterize their chemical composition, structure and magnetic properties.

2. Experimental

The starting reagents were analytical grade $Ba(NO_3)_2$, $Sr(NO_3)_2$, $Fe(NO_3)_3{\cdot}9H_2O$ and citric acid. Organic acid and metal nitrates with molar ratio of 1.4:1 were dis-

* Corresponding author.
E-mail address: shenxq@ujs.edu.cn (X. Shen).

0925-8388/$ – see front matter © 2010 Elsevier B.V. All rights reserved.
doi:10.1016/j.jallcom.2010.07.184

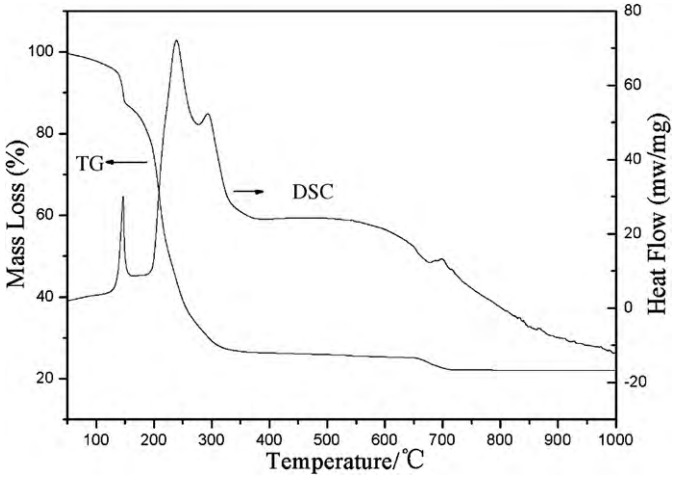

Fig. 1. TG–DSC curves of the gel precursor for $Ba_{0.5}Sr_{0.5}Fe_{12}O_{19}$ ferrite hollow fibers.

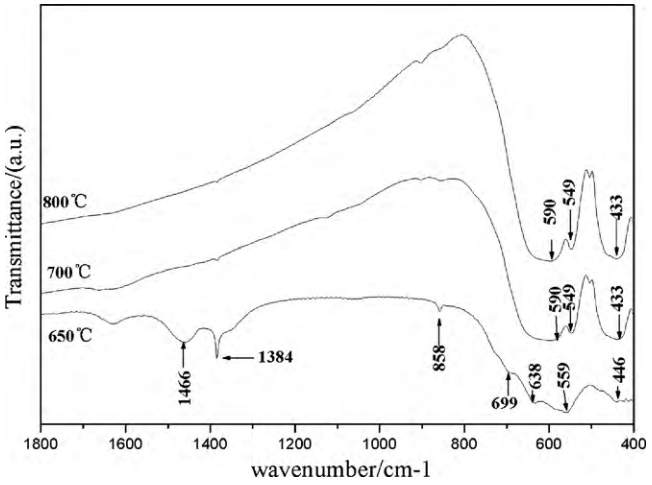

Fig. 2. FTIR spectra of the samples derived from calcination of $Ba_{0.5}Sr_{0.5}Fe_{12}O_{19}$ ferrite precursor at various temperatures.

solved in deionized water to form aqueous solutions with a continuous magnetic stirring. The final solution was magnetically stirred for 20–24 h at room temperatures and was transferred to a rotary evaporator and evaporated in a vacuum at 60–70 °C to remove surplus water until a viscous liquid was obtained. The gel fibers were drawn from the gels with the drawing device and dried in a vacuum oven at 80 °C for about 24 h. The dried gel fibers were then put in an alumina crucible and subsequently were calcined at different temperatures for 2 h under an ambient atmosphere to form the ferrite fibers.

Thermo-gravimetric and scanning calorimetry (TG–DSC) was carried out on a Perkin-Elemer Pyris Diamond TG–DSC thermal analyzer at a heating rate of 10 °C/min under air atmosphere. The X-ray diffraction (XRD) patterns were collected on a Rigaku D/Mmax2500PC diffractometer with Cu-Kα radiation (the wavelength λ = 0.154 nm). Fourier transform infrared spectroscopy (FTIR) spectra of the samples (as pellets in KBr) were recorded by a Nexu670 spectrometer in a wavenumber range of 400–4000 cm^{-1} at a resolution of 4 cm^{-1}. Field emission scanning electron microscopy (FESEM, JSM-7001F) was used to characterize the morphologies of the precursor and calcined ferrite fibers. The magnetic properties of the resultant fibers were investigated at room temperature using a vibrating sample magnetometer (VSM, HH-15) with a maximum applied field of 1194 kA/m (15 kOe).

3. Results and discussion

3.1. Thermal decomposition of gel precursor

Fig. 1 shows the TG–DSC curves of the gel precursor for the $Ba_{0.5}Sr_{0.5}Fe_{12}O_{19}$ ferrite hollow fibers and the thermal decomposition process consists of the following three stages.

The first stage takes place from 50 to 160 °C, and an exothermic peak occurs at around 145 °C, with a corresponding weight loss of 12.5%. At this stage, the free and absorbed water is removed and the gel precursor is broken down.

The second stage is in the range of 160–400 °C. Two exothermic peaks at around 248 and 296 °C on the DSC curve are accompanied by a weight loss about 59.1%, which can be attributed to the initial decomposition of the complexes and a spontaneous combustion. The spontaneous combustion occurs by interactions of citrate and nitrate ions in the gel, with liberation of H_2O, CO_2, NO_x and formation of some metal oxides [18,19].

The third stage is at the temperature range of 400–700 °C. During the early period of this stage 400–650 °C, the $SrCO_3$ and $BaCO_3$ can be formed by the reaction of the metal oxides and CO_2 produced by a continuous oxidization of the organic matters and these carbonates would be decomposed at about 670 °C due to a small endothermic event observed on the DSC curve, corresponding a weigh loss of about 3.5%. When the temperature over about 700 °C, there is almost no mass change on the TG curve, implying the thermal decomposition completed.

3.2. FTIR spectra and XRD analysis

Fig. 2 shows the FTIR spectra for samples derived from calcination of the $Ba_{0.5}Sr_{0.5}Fe_{12}O_{19}$ ferrite precursor at 650, 700 and 800 °C. The XRD patterns of the products derived from calcination of the $Ba_{0.5}Sr_{0.5}Fe_{12}O_{19}$ ferrite precursor at different temperatures are shown in Fig. 3. After calcined at 650 °C, as shown in Fig. 2, the absorption bands at 699, 638, 559 and 446 cm^{-1} can be assigned to γ-Fe_2O_3 and 1466, 1384 and 858 cm^{-1} owing to carbonates [20,21]. The γ-Fe_2O_3 (JCPDS 25-1402), $BaCO_3$ (JCPDS 37-0755) and $SrCO_3$ (JCPDF 05-0418) phases are proved by the XRD reflections for the sample obtained at 650 °C (Fig. 3). When the calcination temperature at 700 and 800 °C, the characteristic bands for the carbonates are no longer detected, while bands at 590, 549 and 433 cm^{-1} occur, which are related to the hexagonal ferrite. From Fig. 3, it can be seen that all the diffraction peaks for the samples calcined at 700–1100 °C are indexed to the magnetoplumbite structure, indicating the single phase $Ba_{0.5}Sr_{0.5}Fe_{12}O_{19}$ ferrite (JCPDS 51-1879) formed. With the calcination temperature increase, the diffraction peaks become narrower and higher, and the crystallization is improved. The average crystallite size (D) can be calculated from the value of full-width at half-maximum (FWHM) of the prominent reflection (1 1 4) using the Scherrer's equation (i.e., $D = 0.89\lambda/(\beta \cos\theta)$, where λ is the wavelength of the X-ray radiation, β is the FWHM of relevant diffraction peak and θ is the Bragg angle.), and the calculated D values of all samples are

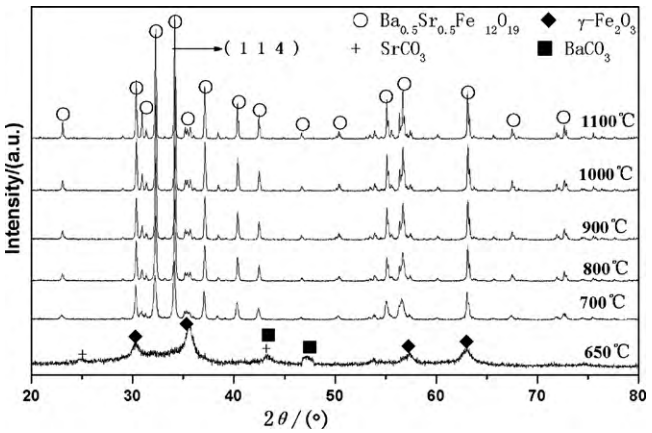

Fig. 3. XRD patterns of the samples derived from calcination of $Ba_{0.5}Sr_{0.5}Fe_{12}O_{19}$ ferrite precursor at different temperatures.

Table 1
Average crystallite size (D) and magnetic parameters of $Ba_{0.5}Sr_{0.5}Fe_{12}O_{19}$ ferrite hollow fibers calcined at different temperatures for 2 h.

Calcination temperature (°C)	D (nm)	M_s (A m^2/kg)	H_c (kA/m)
700	32.6	42.6	305.1
800	37.9	59.8	330.5
900	55.8	64.2	362.9
1000	59.2	63.9	416.5
1100	71.1	64.2	336.2

listed in Table 1. The average crystalline grain size increases from 32.6 to 71.1 nm corresponding to the calcination temperature from 700 to 1100 °C.

Fig. 4 shows the XRD patterns of the $Ba_xSr_{1-x}Fe_{12}O_{19}$ (x = 0–1) ferrite hollow fibers obtained at 1000 °C for 2 h. All the XRD peaks belong to the single phase hexagonal ferrite, which is a solid solution. However, with the barium substitution of strontium, x = 0–1.0, these reflections shift to a lower angle arising from larger barium ions (radius 0.0278 nm) replacing strontium ions (radius 0.0245 nm).

3.3. Morphology of $Ba_xSr_{1-x}Fe_{12}O_{19}$ ferrite hollow fibers

The SEM morphologies of the $Ba_{0.5}Sr_{0.5}Fe_{12}O_{19}$ ferrite hollow fibers obtained at 1000 °C for 2 h are shown in Fig. 5. It can be observed that the $Ba_{0.5}Sr_{0.5}Fe_{12}O_{19}$ ferrite hollow fibers are characterized with thin diameters about 1 μm, a high aspect ratio and a porous structure (Fig. 5a). Fig. 5b shows that the ratio of the hollow diameter to the fiber diameter is estimated about 1/2 from the cross-sections. The $Ba_{0.5}Sr_{0.5}Fe_{12}O_{19}$ ferrite hollow fibers are composed with homogeneous hexagonal plate-like particles with particle sizes below about 100 nm, which is basically consistent with the estimated D value from the corresponding XRD data (Table 1).

Fig. 6 shows the morphologies of the $Ba_xSr_{1-x}Fe_{12}O_{19}$ ferrite hollow fibers with various barium substitutions calcined at 1000 °C for 2 h. These fibers fabricated of fine particles possess a uniform diameter around 2 μm and high aspect ratios. The $Ba_xSr_{1-x}Fe_{12}O_{19}$ ferrite particles, which build the fiber, characterize a homogeneous hexagonal plate-like morphology. Comparing the fiber surface characteristics as shown in Fig. 6, the pores gradually become more with the Ba content increasing from 0 to 0.4, possibly reaching a maximum porosity at the Ba content around 0.5. Then, with the barium content increase further, the surface porosity decreases, as shown in Fig. 6d–f.

3.4. Magnetic property of $Ba_xSr_{1-x}Fe_{12}O_{19}$ ferrite hollow fibers

The hystersis loop measurement was made to determine the magnetic parameters such as the specific saturation magnetization (M_s) and coercivity (H_c). The M_s and H_c values of the $Ba_{0.5}Sr_{0.5}Fe_{12}O_{19}$ ferrite hollow fibers calcined at different temperatures for 2 h are showed in Table 1. With the calcination temperature from 700 to 1100 °C and the grain size of $Ba_{0.5}Sr_{0.5}Fe_{12}O_{19}$ ferrite increasing from 32.6 to 71.1 nm, the coercivity initially increases, reaching a maximum value of 416.5 kA/m at the grain size of 59.2 nm and then exhibits a reduction tendency with the grain size further increase. While the specific saturation magnetization exhibits a different behavior from the coercivity, it increases dramatically from about 42.6 to 64.2 Am^2/kg in the grain size range of 32.6–55.8 nm corresponding the calcination temperature ranging 700–900 °C, and with a further increase of grain size M_s almost maintains the value around 64.2 A m^2/kg.

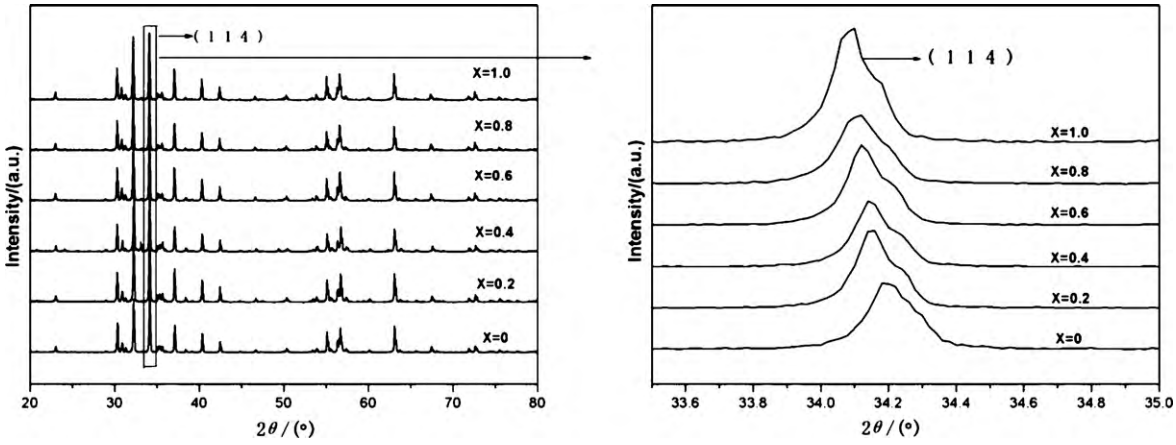

Fig. 4. XRD patterns of $Ba_xSr_{1-x}Fe_{12}O_{19}$ (x = 0–1) ferrites calcined at 1000 °C for 2 h.

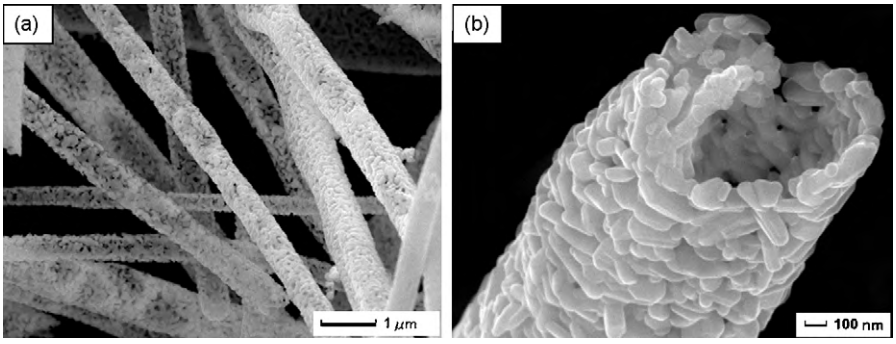

Fig. 5. SEM morphologies of $Ba_{0.5}Sr_{0.5}Fe_{12}O_{19}$ ferrite hollow fibers obtained at 1000 °C for 2 h.

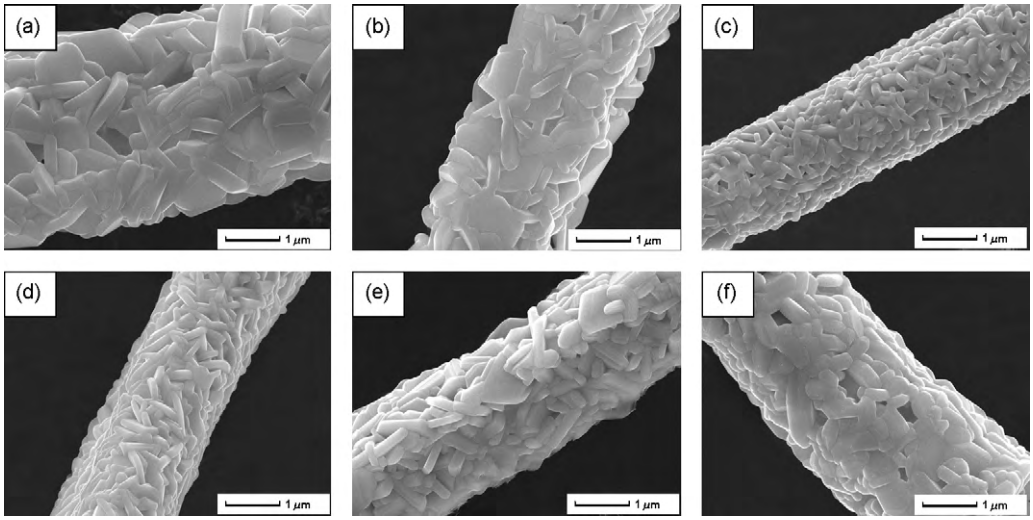

Fig. 6. Surface morphologies of $Ba_xSr_{1-x}Fe_{12}O_{19}$ ferrite hollow fibers with different barium substitutions: (a) $x = 0$, (b) $x = 0.2$, (c) $x = 0.4$, (d) $x = 0.6$, (e) $x = 0.8$, and (f) $x = 1.0$.

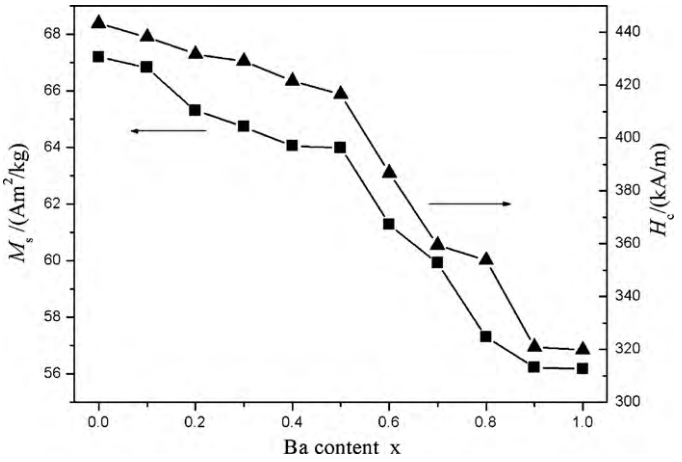

Fig. 7. Effect of barium substitution on M_s and H_c of $Ba_xSr_{1-x}Fe_{12}O_{19}$ ferrite hollow fibers calcined at 1000 °C for 2 h.

According to Stoner–Wohlfarth single-domain theory [22], the magneto-crystalline anisotropy energy (E_A) of a nanocrystal is approximated by

$$E_A = KV \sin^2 \theta$$

where K is the magneto-crystalline anisotropy constant, V is the volume of nanocrystal, and θ is the angle between the ease axis and the direction of field-induced magnetization. H_c is closely related to E_A, which is proportional to the grain size. The H_c value of the $Ba_{0.5}Sr_{0.5}Fe_{12}O_{19}$ ferrite hollow fibers (Table 1) initially increases with the grain size up to 59.2 nm due to the increase in magneto-crystalline anisotropy. When calcined at 1000 °C and over, the grain size of the $Ba_{0.5}Sr_{0.5}Fe_{12}O_{19}$ ferrite hollow fibers may be larger than the single-domain size and become into multi-domains, which change the magnetization mechanism from the magnetic moment reversal to domain wall movement, causing the coercivity to decrease [23]. It can be estimated that the single-domain size of the $Ba_{0.5}Sr_{0.5}Fe_{12}O_{19}$ ferrite hollow fibers is around 60 nm, which is close to the value reported in literatures for the hexagonal ferrite particles [24–26].

The relation of specific saturation magnetization (M_s) and coercivity (H_c) for the $Ba_xSr_{1-x}Fe_{12}O_{19}$ ferrite hollow fibers with barium substitution of strontium is shown in Fig. 7. It can be seen that both the M_s and H_c values of the $Ba_xSr_{1-x}Fe_{12}O_{19}$ ferrite hollow fibers exhibit a continuous decrease from 67.1 A m^2/kg and 443.3 kA/m (for the simple $SrFe_{12}O_{19}$ ferrite, $x = 0$) to 56.1 A m^2/kg and 319.8 kA/m (for the simple $BaFe_{12}O_{19}$ ferrite, $x = 1.0$), respectively. With the addition of barium content in the solid solution, the Ba^{2+} ions having a larger radius and a smaller magnetic moment replace Sr^{2+} ions and occupy the B sites of hexahedron, which will enlarge the distance of Fe–O and effectively reduce the net magnetic moment and the super-exchange. This reduction in the net magnetic moment and super-exchange would result in the decrease of M_s and H_c values with the barium substitution of strontium [27,28].

4. Conclusion

The $Ba_xSr_{1-x}Fe_{12}O_{19}$ ($x = 0$–1) ferrite hollow fibers have been successfully prepared by the gel-precursor transformation method using citric acid and metal salts. The ferrite phase transformation process consists of the gel-precursor thermal decomposition and ferrite phase formation. The $Ba_xSr_{1-x}Fe_{12}O_{19}$ ($x = 0$–1) ferrites are of a solid solution with the magnetoplumbite structure formed at 700 °C. The $Ba_xSr_{1-x}Fe_{12}O_{19}$ ferrites hollow fibers with diameters 1–2 μm have an obvious hollow structure, the ratio of the hollow diameter to the fiber diameter estimated about 1/2. The $Ba_xSr_{1-x}Fe_{12}O_{19}$ ferrite particles, which build the fiber, possess a hexagonal plate-like morphology and grow with the calcination temperature. The magnetic properties are mainly influenced by the grain size and chemical composition. With the barium substitution, the M_s and H_c values of the $Ba_xSr_{1-x}Fe_{12}O_{19}$ ferrite hollow fibers decrease from 67.1 A m^2/kg and 443.3 kA/m (for the simple $SrFe_{12}O_{19}$ ferrite, $x = 0$) to 56.1 A m^2/kg and 319.8 kA/m (for the simple $BaFe_{12}O_{19}$ ferrite, $x = 1.0$), respectively. The $Ba_{0.5}Sr_{0.5}Fe_{12}O_{19}$ ferrite hollow fibers calcined at 1000 °C for 2 h are composed of single-domain grains around 60 nm and exhibit M_s 63.9 A m^2/kg and H_c 416.5 kA/m.

Acknowledgements

This work was financially supported by the National Natural Science Foundation of China (Grant No. 50674048) and Aviation Science Foundation (Grant No. 2009ZF52063).

References

[1] R.C. Pullar, A.K. Bhattacharya, Mater. Lett. 57 (2002) 537–542.
[2] X.F. Yang, Q.L. Li, J.X. Zhao, J. Alloys Compd. 475 (2009) 312–315.

[3] D. Joonghoe, E.K. Lee, J.Y. Park, J. Magn. Magn. Mater. 285 (2005) 164–168.
[4] S.K. Nataraj, B.H. Kim, D.C. Marilou, Mater. Lett. 63 (2009) 218–220.
[5] C.L. Shao, H.Y. Guan, Y.C. Liu, J. Solid State Chem. 177 (2004) 2628–2631.
[6] M.M. Hessien, M.H. Khedr, Mater. Res. Bull. 42 (2007) 1242–1250.
[7] M.C. Dimri, S.C. Kashyap, D.C. Dube, Ceram. Int. 30 (2004) 1623–1626.
[8] H.F. Yu, P.C. Liu, J. Alloys Compd. 416 (2006) 222–227.
[9] P. Shepherd, K.K. Mallick, R.J. Green, J. Magn. Magn. Mater. 311 (2007) 683–692.
[10] E.A. Gravchikova, D.D. Zaitsev, P.E. Kazin, J. Inorg. Mater. 42 (2006) 914–917.
[11] P. Xu, X.J. Han, M.J. Wang, J. Phys. Chem. C 111 (2007) 5866–5870.
[12] D.H. Chen, Y.Y. Chen, J. Colloid Interf. Sci. 236 (2001) 41–46.
[13] I.P. Parkin, Q.A. Pankhurst, G. Elwin, Adv. Mater. 8 (1997) 643–645.
[14] D. Barb, L. Diamandescu, A. Rusi, J. Mater. Sci. 21 (1986) 1118–1122.
[15] A. Ataie, I.R. Harris, C.B. Ponton, J. Mater. Sci. 30 (1995) 1429–1433.
[16] C. Gong, G. Fan, C. Song, Trans. Tianjin Univ. 13 (2007) 117–120.
[17] R.C. Pullar, A.K. Bhattacharya, J. Magn. Magn. Mater. 300 (2006) 490–499.
[18] Z. Yue, J. Zhou, L. Li, H. Zhang, Z. Gui, J. Magn. Magn. Mater. 208 (2000) 55–60.
[19] K.H. Wu, C.H. Yu, Y.C. Chang, D.N. Horng, J. Solid State Chem. 177 (2004) 4119–4125.
[20] A. Mali, A. Ataie, Scripta Mater. 53 (2005) 1065–1070.
[21] H.F. Yu, H.Y. Lin, J. Magn. Magn. Mater. 283 (2004) 190–198.
[22] E.C. Stoner, E.P. Wohlfarth, IEEE Trans. Magn. 27 (1991) 3475–3518.
[23] J.H. Choy, Y.S. Han, S.W. Song, Mater. Lett. 19 (1994) 257–262.
[24] C.S. Lin, C.C. Hwang, T.H. Huang, Mater. Sci. Eng. B 139 (2007) 24–36.
[25] C. Sürig, K.A. Hempel, D. Bonnenberg, Appl. Phys. Lett. 63 (1993) 2386–2389.
[26] S.D. Kulkarni, S.R. Sainkar, S.K. Date, Appl. Phys. Lett. 68 (1996) 3491–3495.
[27] M.J. Iqbal, S. Farooq, Mater. Chem. Phys. 118 (2009) 308–313.
[28] D.M. Hemeda, A. Al-Sharif, O.M. Hemeda, J. Magn. Magn. Mater. 315 (2007) L1–L7.